

Interstellar Isomers: The Importance of Bonding Energy Differences

Anthony J. Remijan^{1,2}, J. M. Hollis¹, F. J. Lovas³,
D. F. Plusquellic³ & P. R. Jewell⁴

ABSTRACT

We present strong detections of methyl cyanide (CH_3CN), vinyl cyanide (CH_2CHCN), ethyl cyanide ($\text{CH}_3\text{CH}_2\text{CN}$) and cyanodiacetylene (HC_4CN) molecules with the Green Bank Telescope (GBT) toward the Sgr B2(N) molecular cloud. Attempts to detect the corresponding isocyanide isomers were only successful in the case of methyl isocyanide (CH_3NC) for its $J_K = 1_0 - 0_0$ transition, which is the first interstellar report of this line. To determine the spatial distribution of CH_3NC , we used archival Berkeley-Illinois-Maryland Association (BIMA) array data for the $J_K = 4_K - 3_K$ ($K = 0 - 3$) transitions but no emission was detected. From ab initio calculations, the bonding energy difference between the cyanide and isocyanide molecules is $>8500 \text{ cm}^{-1}$ ($>12,000 \text{ K}$). Thus, cyanides are the more stable isomers and would likely be formed more preferentially over their isocyanide counterparts. That we detect CH_3NC emission with a single antenna (Gaussian beamsize(Ω_B)= 1723 arcsec^2) but not with an interferometer ($\Omega_B=192 \text{ arcsec}^2$), strongly suggests that CH_3NC has a widespread spatial distribution toward the Sgr B2(N) region. Other investigators have shown that CH_3CN is present both in the LMH hot core of Sgr B2(N) and in the surrounding medium, while we have shown that CH_3NC appears to be deficient in the LMH hot core. Thus, large-scale, non-thermal processes in the surrounding medium may account for the conversion of CH_3CN to CH_3NC while the LMH hot core, which is dominated by thermal processes, does not produce a significant amount of CH_3NC . Ice analog experiments by other investigators have shown that radiation bombardment of CH_3CN can produce CH_3NC , thus supporting our observations. We

¹NASA Goddard Space Flight Center, Computational and Information Sciences and Technology Office, Code 606, Greenbelt, MD 20771

²National Research Council Resident Research Associate

³Optical Technology Division, National Institute of Standards and Technology, Gaithersburg, MD 20899

⁴National Radio Astronomy Observatory, P. O. Box 2, Green Bank, WV 24944-0002

conclude that isomers separated by such large bonding energy differences are distributed in different interstellar environments, making the evaluation of column density ratios between such isomers irrelevant unless it can be independently shown that these species are co-spatial.

Subject headings: ISM: abundances - ISM: clouds - ISM: individual (Sagittarius B2(N)) - ISM: molecules - radio lines: ISM

1. INTRODUCTION

The observations of isomers in the interstellar medium is becoming increasingly more common as new and larger molecules are being detected. Currently, 135 molecules have been detected in interstellar and circumstellar environments. Excluding diatomic molecules, $\sim 30\%$ of all interstellar molecules have observed isomeric counterparts. In addition, as the number of atoms in an interstellar molecule increases, so do the number of isomers. For example, of the 9 interstellar molecules containing 8 atoms, 5 are isomers. With an empirical formula $C_2H_4O_2$, acetic acid (CH_3COOH), glycolaldehyde (CH_2OHCHO) and methyl formate (CH_3OCHO) are isomers; and for H_2C_6 , hexapentaenylidene and triacetylene (HC_6H) are isomers. Isomerism may provide important clues to the formation of interstellar molecules. As such, an important class of isomers are cyanide ($-CN$) and isocyanide ($-NC$) species.

Hydrogen cyanide (HCN), methyl cyanide (CH_3CN), vinyl cyanide (CH_2CHCN), and ethyl cyanide (CH_3CH_2CN) all have large abundances and are easily detectable in a number of interstellar environments and are readily seen in the spectra of several molecular line surveys (e.g. Friedel et al. 2004, Nummelin et al. 1998). However, while there have been detections of HNC in interstellar and cometary environments, there have been no confirmed detection of the isocyanides CH_3NC , CH_2CHNC , and CH_3CH_2NC . The first tentative detection of CH_3NC was toward Sgr B2(OH) by Cernicharo et al. (1988) from observations of the $J = 4 - 3$, $J = 5 - 4$, and $J = 7 - 6$ transitions. Though the lines were highly contaminated from other known interstellar species, they calculated an CH_3NC/CH_3CN abundance ratio of $\sim 0.03-0.05$. Since this initial claim, there have been no further observations to confirm the existence of interstellar CH_3NC , in particular toward the LMH hot core of Sgr B2(N), the best known source of large molecules. Thus, in this work, we confirmed the existence of CH_3NC and attempted to observe other large isocyanides by observing the same (or similar) low energy transitions of the cyanides CH_3CN , CH_2CHCN , CH_3CH_2CN , and HC_4CN

and their corresponding isocyanide isomers toward the the high-mass star forming region, Sgr B2(N).

2. OBSERVATIONS AND RESULTS

The observations using the NRAO 100-m Robert C. Byrd Green Bank Telescope (GBT) were made in 2004 February 24, February 29 and March 29. Table 1 lists the molecular line parameters of the transitions of the cyanides and isocyanides sought. The species, calculated rest frequencies, transition quantum numbers, line strengths, upper level energies, and continuum levels are listed in the first six columns of Table 1. The GBT half-power beamwidth (θ_B) is given as $740''/\nu$ [GHz]. The K-band receiver set used has a frequency range covering 18 GHz to 22.5 GHz. For the observations reported herein, the average beamwidth $\langle \theta_B \rangle = 39''$ corresponds to an average Gaussian beamsize of $\langle \Omega_B \rangle = \pi \theta_B^2 / [4 \ln(2)] = 1723 \text{ arcsec}^2$ and an average beam efficiency $\langle \eta_B \rangle \sim 0.8$. The GBT spectrometer was configured in its 8 intermediate frequency (IF), 200 MHz, 3-level mode which permits observing four 200 MHz frequency bands at a time in two polarizations through the use of offset oscillators in the IF. This mode affords 24.4 kHz channel separation. Antenna temperatures are on the T_A^* scale (Ulich & Haas 1976) with estimated 20% uncertainties. The Sgr B2(N-LMH) J2000 pointing position employed was $\alpha = 17^h 47^m 19^s.8$, $\delta = -28^\circ 22' 17''$ and the LMH systemic LSR source velocity of $+64 \text{ km s}^{-1}$ was assumed. Automatically updated dynamic pointing and focusing corrections were employed based on realtime temperature measurements of the structure input to a thermal model of the GBT; zero points were adjusted typically every two hours or less using the calibrators 1626-298 and/or 1733-130. Data were taken in the OFF-ON position-switching mode, with the OFF position $60'$ east in azimuth with respect to the ON source position. A single observation consisted of two minutes in the OFF source position followed by two minutes in the ON source position. The two polarization outputs from the spectrometer were averaged in the final data reduction process to improve the signal-to-noise ratio.

Figure 1 shows our attempt to detect cyanide and isocyanide species toward Sgr B2(N) with the GBT. The panels in the left column show the detections of CH_3CN , CH_2CHCN , $\text{CH}_3\text{CH}_2\text{CN}$ and HC_4CN . We have successfully detected all species in the left column and for the first time the $J_{K_a, K_c} = 2_{11} - 1_{10}$ transition of interstellar $\text{CH}_3\text{CH}_2\text{CN}$ is reported. In the panels containing the transitions of CH_3CN , CH_2CHCN and $\text{CH}_3\text{CH}_2\text{CN}$, the intensity scale (ordinate) decreases, showing that the emission from the larger species is in general weaker. The abscissa is the radial velocity with respect to the local standard of rest (LSR) calculated for the rest frequency of the transition shown at the top left of each panel assuming a source

velocity of $+64 \text{ km s}^{-1}$. Dashed lines show LSR velocities of $+64$, $+73$ and $+82 \text{ km s}^{-1}$. Molecules with no hyperfine (HF) structure previously observed with the GBT such as propenal (CH_2CHCHO), propanal ($\text{CH}_3\text{CH}_2\text{CHO}$), and glycolaldehyde (CH_2OHCHO) show absorption components at $+64$ and $+82 \text{ km s}^{-1}$ and an emission component at $+73 \text{ km s}^{-1}$ (Hollis et al. 2004a, b). In general, the cyanide spectra shown in the left panel of Figure 1 are consistent with this source velocity structure. In the cases of CH_3CN and CH_2CHCN , however, the source velocity structure is confused by molecular HF splitting. The fiducial on each HF component denotes the position corresponding to $+64 \text{ km s}^{-1}$. Thus, it can be seen that only the $F=0-1$ components are clear of any complication. The panels in the right column of Figure 1 show the passbands containing the transitions of CH_3NC , CH_2CHNC , $\text{CH}_3\text{CH}_2\text{NC}$ and HC_4NC . We clearly detect the absorption and emission components at $+64$, $+73$ and $+82 \text{ km s}^{-1}$ from CH_3NC and there is possible narrow emission from CH_2CHNC near $+64 \text{ km s}^{-1}$. The primary absorption component of CH_3NC at $+64 \text{ km s}^{-1}$ is more than an order of magnitude weaker in intensity than the corresponding feature of CH_3CN , however this is the first interstellar report of this line. No emission or absorption is seen from either $\text{CH}_3\text{CH}_2\text{NC}$ or HC_4NC beyond a 1σ detection limit ($\sim 2 \text{ mK}$).

The $J_K = 4_K - 3_K$ ($K = 0-3$) CH_3NC observations using the Berkeley-Illinois-Maryland Association (BIMA) Millimeter Array¹ were made in 2001 April 20 in its C configuration toward Sgr B2(N-LMH). The pointing position was the same as used for the GBT. Table 2 lists the molecular line parameters of each species in the CH_3NC passband. The species, the calculated rest frequencies, the transition quantum numbers, the product of the line strength and the square of the dipole moment ($S\mu^2$), and the upper level energies are listed in the first five columns of Table 2. The synthesized beamwidth for these observations is $\theta_a \times \theta_b = 23.''9 \times 7.''1$ corresponding to a Gaussian beamsize of $\Omega_B = 192 \text{ arcsec}^2$. The quasar 1733-130 was used to calibrate the antenna based gains and Uranus was used as the flux density calibrator. The absolute amplitude calibration of these sources is accurate to within $\sim 20\%$. The passbands were calibrated automatically during data acquisition; a technical description of auto-calibration can be found at <http://astron.berkeley.edu/~plambeck/technical.html>. The spectral window containing the CH_3NC transitions has a bandwidth of 50 MHz and is divided into 128 channels for a spectral resolution of 0.39 MHz per channel. All data were combined, imaged, and self-calibrated using the MIRIAD software package (Sault, Teuben & Wright 1995).

Figure 2 shows fiducials for the $J_K = 4_K - 3_K$ ($K = 0 - 3$) transitions of CH_3NC in a passband dominated by strong emission from $\text{CH}_3\text{CH}_2\text{CN}$ which is largely confined to the LMH hot core (Liu & Snyder 1999). The rest frequency located in the upper left of the panel

¹Operated by the University of California, Berkeley, the University of Illinois, and the University of Maryland with support from the National Science Foundation.

corresponds to the $J_{K_a, K_c} = 9_{28} - 8_{27}$ transition of $\text{CH}_3\text{CH}_2\text{CN}$ for an assumed LSR velocity of $+64 \text{ km s}^{-1}$. Dashed lines denote LSR velocities of $+64$, $+73$ and $+82 \text{ km s}^{-1}$. The transition of $\text{CH}_3\text{CH}_2\text{CN}$ clearly shows strong emission components at the LMH systemic velocity of $+64 \text{ km s}^{-1}$ and also at $+73 \text{ km s}^{-1}$. The $J_K = 4_K - 3_K$ ($K = 0 - 3$) CH_3NC transitions are labeled in this passband assuming an LSR velocity of $+64 \text{ km s}^{-1}$ and, except for the $J_K = 4_3 - 3_3$ transition, all lie in a region that is clear from any other molecular line emission. However, no transition of CH_3NC is detected above a 1σ detection limit ($\sim 0.3 \text{ Jy beam}^{-1}$). The 1σ rms noise level fiducial is shown at the left of the panel.

3. DISCUSSION

We have presented two disparate sets of observations: GBT single antenna results with a Gaussian beamsize of $\Omega_B = 1723 \text{ arcsec}^2$, and BIMA array results obtained with a Gaussian beamsize of $\Omega_B = 192 \text{ arcsec}^2$. Given the GBT beamsize is a factor of 9 greater than the BIMA beamsize, the spatial scale of the GBT will couple better to the extended emission toward Sgr B2(N). Conversely, the BIMA array will tend to couple better to the 28 arcsec^2 ($\sim 5''$ diameter) of the LMH hot core. Hence, we expect that the GBT observations will be characterized by a lower excitation temperature (T_{ex}) than the excitation temperature associated with the BIMA observations. First, we will derive the cyanide and isocyanide column densities from the GBT observations. Then, we will show from BIMA observations that CH_3NC must be extended.

For the GBT observations, following the formalism outlined in Hollis et al. (2004b), the total beam-averaged column density of a molecular species obtained with a single element radio telescope is given as:

For emission:

$$N_T = (1.8 \times 10^{14}) \frac{Q_r e^{E_u/T_{ex}}}{\nu S \mu^2} \frac{\left\{ \frac{\Delta T_A^* \Delta V}{\eta_B} \right\}}{\left\{ 1 - \frac{(e^{(4.8 \times 10^{-5})\nu/T_{ex}} - 1)}{(e^{(4.8 \times 10^{-5})\nu/T_{bg}} - 1)} \right\}} \text{ cm}^{-2}. \quad (1)$$

For absorption:

$$N_T = (8.5 \times 10^9) \frac{Q_r \left\{ \frac{\Delta T_A^* \Delta V}{\eta_B} \right\}}{\left\{ T_{ex} - \frac{T_c}{\eta_B} \right\} S \mu^2 \{ e^{-E_l/T_{ex}} - e^{-E_u/T_{ex}} \}} \text{ cm}^{-2}. \quad (2)$$

In both equations, the line shapes are assumed to be Gaussian; η_B is the telescope beam efficiency; T_{ex} is the excitation temperature; $\Delta T_A^* \Delta V$ is the product of the fitted line intensity (mK) and line width (km s^{-1}); Q_r is the rotational partition function; $S\mu^2$ is the product of the transition line strength and the square of the dipole moment (Debye²); and E_u is the upper rotational energy level (K). In equation (1), ν is the transition frequency (MHz) and $T_{bg} \sim 2.7$ K is the cosmic background temperature. In equation (2), T_c is the source continuum temperature (K), and E_l is the lower rotational energy level (K).

Using the GBT at K-band, Hollis et al. (2004b) found a glycolaldehyde excitation temperature of $T_{ex}=8$ K that satisfied the detected integrated line intensities of the absorption components at +64 and +82 km s^{-1} and the emission component at +73 km s^{-1} . Since the LSR velocity components of the cyanide and isocyanide molecules in Figure 1 appear to be similar, we used $T_{ex}=8$ K to find the total column density of each of the detected species. Columns (7) to (12) of Table 1 summarize the Gaussian fitting intensities and line widths for each detected transition or 3 σ upper limits for the intensities of non-detections at LSR velocities of +64, +73 and +82 km s^{-1} .

In order to determine the intensity and line width of the individual HF and velocity components of the CH_3CN and CH_2CHCN lines, multiple Gaussian fits were used. By fixing the frequency separation between HF components, we fit the +64, +73 and +82 km s^{-1} velocity components for each HF component. If the fitting routine found a solution for the intensity of a velocity component less than the 3 σ rms noise level, it was omitted, and the fit recalculated for one less velocity component. The results are listed in columns 7-12 of Table 1. In Figure 1a, the solid line is the result of Gaussian fitting the 3 HF structure components to the +64, +73 and +82 km s^{-1} LSR velocity structure (see Table 1). Furthermore, as a residual to this methodology, the small absorption dip near 50 km s^{-1} in Figure 1a is not due to a HF component nor is it a velocity component of CH_3CN .

The column densities listed in column (13) of Table 1 are the sum of all detected velocity components, or, in the cases of CH_3CN and CH_2CHCN , of all velocity and HF components. The column densities of the cyanide molecules are within a factor of 3 or 4 of the CH_3CN column density of ($\sim 10^{14} \text{ cm}^{-2}$). Furthermore, the column density measured from the +64 km s^{-1} velocity component accounts for $\sim 75\%$ of the total CH_3CN column density. The +64 km s^{-1} velocity component is often the only one resolved at higher frequencies and is the basis for the majority of CH_3CN column density measurements at 1 and 3 mm wavelengths.

The similarity in column densities between cyanides is also seen at higher resolution toward other sources (Remijan et al. 2004b). The column density ratio $\text{CH}_3\text{NC}/\text{CH}_3\text{CN}$ is ~ 0.02 and is relevant if and only if the two species are co-spatial. The possible detection of

CH₂CHNC gives a column density ratio CH₂CHNC/CH₂CHCN of ~ 0.005 .

From Remijan et al. (2003), the total beam averaged column density obtained with an interferometer is:

$$N_T = 2.04 \times \frac{\int \Delta I dv Q_r e^{(E_u/T_{ex})}}{B \theta_a \theta_b \nu^3 S \mu^2} \times 10^{20} \text{ cm}^{-2}. \quad (3)$$

In equation (3), $\int \Delta I dv$ is the product of the fitted line intensity (Jy beam⁻¹) and line width (km s⁻¹), θ_a and θ_b are the FWHM beam widths (arcsec) and $B = \Omega_S / [\Omega_B + \Omega_S]$ is the beam filling factor where Ω_B is the solid angle subtended by the synthesized beam of the interferometer and Ω_S is the solid angle subtended by the source emission. For the BIMA array data, $\theta_a \times \theta_b = 23.''9 \times 7.''1$. Columns (7) to (12) of Table 2 summarize the Gaussian fitting intensities and line widths for CH₃CH₂CN and the 3 σ upper limits for the intensities of the non-detections at LSR velocities of +64, +73 and +82 km s⁻¹. The column density of CH₃CH₂CN in column (13) is based on the excitation temperature of methanol (CH₃OH) of 170 K (Pei, Liu & Snyder 2000).

No emission for the $J = 4 - 3$ ($K = 0 - 3$) transition of CH₃NC was seen in the BIMA array SgrB2(N) data. However, if CH₃NC and CH₃CN are co-spatial (i.e., our GBT CH₃NC/CH₃CN ratio of ~ 0.02 is valid), then observations of CH₃CN by other investigators which yield large CH₃CN column densities predict that we should have detected CH₃NC with the BIMA Array if the source is compact. In an extensive survey encompassing the $J = 12 \rightarrow 11$, $J = 13 \rightarrow 12$ and $J = 14 \rightarrow 13$ transitions of CH₃CN at 1 mm wavelengths, Nummelin et al. (2000) obtained a CH₃CN beam averaged column density of $\sim 4.2 \times 10^{15} \text{ cm}^{-2}$ for a 352 K LMH hot core temperature. These observations were performed using the 15m SEST telescope with a $\sim 600 \text{ arcsec}^2$ beamsize. Owing to the lower spatial resolution ($\sim 2 \text{ km s}^{-1} \text{ channel}^{-1}$) at 1 mm wavelengths and the large line widths (15-20 km s⁻¹) of CH₃CN lines toward Sgr B2(N-LMH) (Nummelin et al. 2000), it is not possible to resolve the individual velocity components of the CH₃CN lines. Thus, the calculated column density is based solely on the +64 km s⁻¹ LSR velocity component. In addition to the the column density and temperature, Nummelin et al. also found a beam filling factor of the CH₃CN emission toward the Sgr B2(N) hot core of 0.014. In their data analysis, the column density, rotational temperature and beam filling factor were given as free parameters. From these values, an integrated line intensity was calculated for each transition and was compared to the observed integrated line intensity until a “best-fit” model was obtained. The best-fit model was found by finding the minimum of the reduced χ^2 function (Nummelin et al. 2000). Assuming the model explains the physics accurately, the measured values of the rotational temperature, column density and beam filling factor by Nummelin et al. toward

the Sgr B2(N) hot core are reported at a 68.3% confidence interval (1σ). Given the ~ 600 arcsec² beamsizes of the 15m SEST telescope, and a beam filling factor of 0.014, the measured source size of the CH₃CN emitting region toward the Sgr B2(N) hot core is ~ 8.5 arcsec². This size is very similar to the CH₃CN cores toward W51e1 (7.9(6)arcsec²) and W51e2 (6.0(9)arcsec²) (Remijan et al. 2004a). Furthermore, the size is also similar to the emitting regions of CH₂CHCN and CH₃CH₂CN towards the Sgr B2(N) hot core measured by Liu & Snyder (1999) at subarcsecond resolution. Thus, ~ 8.5 arcsec² is a reasonable measure of the CH₃CN emitting region toward the Sgr B2(N) hot core. Using the measured rotational temperature of 352 K, the scaled Nummelin et al. (2000) CH₃CN column density within the 192 arcsec² beamsizes of the BIMA array is $\sim 9.9 \times 10^{16}$ cm⁻². Using the column density ratio of 0.02, the expected CH₃NC column density of the +64 km s⁻¹ LSR velocity component should be $\sim 2 \times 10^{15}$ cm⁻² for co-spatial isomers.

Solving equation (3) for $\int \Delta I dv$ assuming a column density of $\sim 2 \times 10^{15}$ cm⁻², we should have detected a CH₃NC integrated line intensity of ~ 57 Jy beam⁻¹ km s⁻¹ for the $J_K = 4_0 - 3_0$ transition. Assuming a typical line width of 15 km s⁻¹ for the LMH hot core of Sgr B2(N), the expected peak intensity of the $4_0 - 3_0$ transition is ~ 3.8 Jy beam⁻¹. However, the BIMA array data shows no CH₃NC emission greater than the 1σ rms upper limit of ~ 0.3 Jy beam⁻¹. The most likely explanation for the lack of a CH₃NC detection is that the emission is extended and the array cannot couple to it. In the case of extended emission, the ratio of the measured line intensity, or in our case the 1σ rms upper limit of ~ 0.3 Jy beam⁻¹, to the expected line intensity of ~ 3.8 Jy beam⁻¹ is equal to the ratio of the solid angle subtended by the synthesized beam of the interferometer (Ω_B) to the solid angle subtended by the source emission (Ω_S). This is because the synthesized beam of the interferometer is only collecting a fraction of the flux from the extended emission region which we assume to be uniformly distributed. Therefore our observations indicate that $\Omega_B/\Omega_S < 0.3/3.8$. Solving for the source size assuming a Gaussian beamsizes of 192 arcsec², we find $\Omega_S > 2432$ arcsec² or equivalently, a linear size of $> 100''$ (1.7'), which is much larger than the typical LMH hot core diameter of $\sim 5''$ (Hollis et al. 2003). This strongly suggests that the spatial distribution of CH₃NC is extended and would not show any significant concentration toward the LMH hot core.

DeFrees, McLean, & Herbst (1985) theoretically calculated a CH₃NC/CH₃CN abundance ratio for dense interstellar clouds in the range of 0.1-0.4 by assuming that both species are formed from ion precursors and destroyed by gas phase, ion molecule reactions. The DeFrees et al. calculations show that when CH₃⁺ collides with HCN, a collision complex is formed that rapidly equilibrates to protonated methyl isocyanide (CH₃NCH⁺) and protonated methyl cyanide (CH₃CNH⁺) due to the large amount of energy produced from the initial collision. As the ensemble of ions continues to relax, the internal energy of CH₃CNH⁺

becomes insufficient to overcome the barrier to isomerize to CH_3NCH^+ . The end result finds CH_3CN formed preferentially over CH_3NC . We performed ab initio calculations in order to quantify the energy differences between cyanide and isocyanide isomers in this work. Table 3 lists each molecular species (col. 1), the zero-point corrected bonding energy (ZPCBE in col. 2) and the relative ZPCBE (col. 3). Column (2) ZPCBE represents the complete dissociation of the molecule into its constituent atoms. Note that the relative bonding energies between isomers are very large ($>8500 \text{ cm}^{-1}$). Thus, the cyanide molecules are much more stable than their isocyanide isomers, and therefore it is highly unlikely that any thermal process can satisfactorily explain the formation of isocyanide molecules. This indicates that a non-thermal process is necessary to convert a cyanide into an isocyanide species.

In recent laboratory experiments performed by Hudson & Moore (2004), cyanide species were bombarded by both protons and UV-photons to determine what would happen to the structure of the molecule. Bombarding a pure ice sample of CH_3CN at 24 K, the proton experiment yielded ketenimine (CH_2CNH), another isomer of CH_3CN , as well as CH_3NC in a slightly lower abundance. Similarly, the UV-photon experiment at 12 K yielded CH_3NC as the primary product. These products were also seen when CH_3CN was embedded in N_2 ice and then irradiated. Hudson & Moore (2004) also note that the temperature in both experiments did not affect the formation of the end products. In an UV-photon experiment performed at 100 K, the destruction of CH_3CN was faster than at 12 K, but the same end products were seen. This suggests that the reactions were driven more by the radiation dose than the sample temperature (Hudson & Moore 2004), reinforcing our suggestion that non-thermal processes may be the primary route to the formation of interstellar isocyanides. Laboratory experiments involving CH_2CHCN , $\text{CH}_3\text{CH}_2\text{CN}$, and cyanoacetylene (HC_2CN), all showed similar results for isocyanide isomers. It is likely that a similar reaction involving HC_4CN will produce HC_4NC . Furthermore, these laboratory experiments also suggest that all isocyanides are likely to be formed under the conditions which interstellar CH_3NC was detected. Based on the column density ratios and upper limits in Table 1, we did not detect any emission from $\text{CH}_3\text{CH}_2\text{NC}$ and HC_4NC because of the possibility that we did not integrate long enough to detect these species. On the other hand, Hudson & Moore (2004) also conducted experiments with cyanides embedded in H_2O ice and found that hydrogen addition and subtraction reactions were taking place in both radiation bombardment reactions in which *no* isocyanides were formed. In these experiments HC_2CN hydrogenated to CH_2CHCN and then to $\text{CH}_3\text{CH}_2\text{CN}$. Based on the aforementioned laboratory results, we will suggest how large cyanides and their corresponding isocyanide isomers may be produced in the extended regions surrounding Sgr B2(N).

The Sgr B2(N) region is known to contain widespread shocks (Chengalur & Kanekar 2003). Such shocks have been presumed to be responsible for the formation and distribution

of large aldehyde molecules toward this region (Hollis et al. 2004a, b). Furthermore, it is also well known that there is ambient UV flux and cosmic ray flux in these regions. On the surfaces and mantles of dust grains, larger species such as CH_3CN and HC_2CN may be present. CH_2CHCN and $\text{CH}_3\text{CH}_2\text{CN}$ are formed as a result of H-addition reactions, thus depleting HC_2CN . As a shock passes, these large molecules are expelled from the grain surface into the gas phase. At this point UV and cosmic rays may interact with the cyanide species and form isocyanides. As a result, the isocyanides show an extended distribution. In hot cores, there is a lower UV and cosmic ray flux due to the large column density of gas and dust. Furthermore, thermal processes are the primary mechanism to liberate molecules off grain surfaces (Tielens & Hagen 1982; Hasegawa, Herbst, & Lueng 1992). Indeed, this is initially why these regions were believed to be the ideal places to form large molecules (Ehrenfreund & Charnley 2000). Also, in these compact regions, it is believed warm gas phase chemistry in addition to grain surface chemistry can form large molecules which may account for the enhanced abundances of CH_2CHCN and $\text{CH}_3\text{CH}_2\text{CN}$ in hot core regions (Liu & Snyder 1999, see also $\text{CH}_3\text{CH}_2\text{CN}$ column density in Table 2 with respect to Table 1). However, thermal processes are not enough to form isocyanide species after the cyanides have been expelled from the grain and hence there should be a depletion of isocyanides towards hot cores. Our observations support this hypothesis.

In summary, we have calculated the chemical bonding energies for cyanide molecules studied herein (CH_3CN , CH_2CHCN , $\text{CH}_3\text{CH}_2\text{CN}$, & HC_4CN) and found they are much greater ($>8500\text{ cm}^{-1}$) than that of the corresponding isocyanide isomers. As a consequence, cyanide interstellar molecules are most likely preferentially formed at the expense of isocyanide isomers. Moreover, in the case of CH_3CN , it is seen in the LMH hot core and in the surrounding medium while CH_3NC appears to be deficient in the LMH hot core. This suggests that large-scale, non-thermal processes such as shocks or enhanced UV flux in the surrounding medium account for the conversion of CH_3CN to CH_3NC while the LMH hot core is dominated by thermal processes which cannot produce a significant amount of CH_3NC . Hudson & Moore (2004) have shown that radiation bombardment of CH_3CN in ice analog experiments can produce CH_3NC , thus tending to support what is observed. Additionally, since CH_3NC is deficient in the LMH and CH_3CN is prevalent, this suggests that the relative abundance ratio between these two isomers is not meaningful because the molecules are not co-spatial. This may well apply to other cyanide and isocyanide isomers.

J.M.H. gratefully acknowledges research support from H.A. Thronson, Assistant Associate Administrator for Technology, NASA Science Mission Directorate. We also greatly thank an anonymous referee whose comments and suggestions provided additional insight to this manuscript.

REFERENCES

- Alexander, A. J., Kroto, H. W., & Walton, D. R. M. 1976, *J. Mol. Spect.*, 62, 175
- Anderson, R. J. & Gwinn, W. D. 1968, *J. of Chem. Physics*, 49, 3988
- Bauder, A. 1979, *J. Phys. Chem. Ref. Data*, 8, 583
- Bolton, K., Owen, N. L., & Sheridan, J. 1970, *Spectrochim. Acta*, 26A, 909
- Botschwina, P., Heyl, A., Chen, W., McCarthy, M. C., Grabow, J.-U., Travers, M. J., & Thaddeus, P. 1998, *J. Chem. Phys.* 109, 3108
- Boucher, D., Burie, J., Bauer, A., Dubrulle, A., & Demaison, J. 1980, *J. Phys. Chem. Ref. Data*, 9, 659
- Cernicharo, J., Kahane, C., Guelin, M., & Gomez-Gonzalez, J. 1988, *A&A*, 189, L1
- Chengalur, J.N., & Kanekar, N. 2003, *A&A*, 403, L43
- DeFrees, D. J., McLean, A. D., & Herbst, E. 1985, *ApJ*, 293, 236
- Dunning, T. H. Jr. 1989, *J. Chem. Phys.* 90, 1007
- Ehrenfreund, P. & Charnley, S. B. 2000, *ARA&A*, 38, 427
- Fliege, E. & Dreizler, H. 1985, *Z. Naturforsch.*, 40a, 43
- Friedel, D. N., Snyder, L. E., Turner, B. E., & Remijan, A. 2004, *ApJ*, 600, 234
- Frisch et al. 2004, *Gaussian 03*, Revision C.01, Gaussian, Inc., Wallingford CT
- Gadhi, J., Lahrouni, A., Legrand, J., & Demaison, J. 1995, *J. Chim. Phys.*, 92, 1984
- Gerry, M. C. L., Yamada, K., & Winnewisser, G. 1979, *J. Phys. Chem. Ref. Data*, 8, 107
- Ghosh, S. N., Trambarlo, R. & Gordy, W. 1953, *J. Chem. Phys.*, 21, 308
- Hasegawa, T. I., Herbst, E., & Leung, C. M. 1992, *ApJS*, 82, 167
- Hollis, J. M., Pedelty, J. A., Boboltz, D. A., Liu, S.-Y., Snyder, L. E., Palmer, Patrick, Lovas, F. J., & Jewell, P. R. 2003, *ApJ*, 596, 235
- Hollis, J. M., Jewell, P. R., Lovas, F. J., Remijan, A., & Møllendal, H. 2004a, *ApJ*, 610, L21
- Hollis, J. M., Jewell, P. R., Lovas, F. J., & Remijan, A. 2004b, *ApJ*, 613, L45

- Hudson, R. L. & Moore, M. H. 2004, *Icarus*, 172, 466
- Kendall, R. A., Dunning, T. H. Jr., & Harrison, R. J. 1992, *J. Chem. Phys.* 96, 6769
- Killian, T. C., Gottlieb, C. A., Gottlieb, E. W., Vrtilik, J. M., & Thaddeus, P. 1990, *ApJ*, 365, 89
- Kukolich, S. G. 1972, *J. Chem. Physics*, 57, 869
- Liu, S.-Y. & Snyder, L. E. 1999, *ApJ*, 523, 683
- Lovas, F. J. 1982, *J. Phys. Chem. Ref. Data*, 11, 251
- Nummelin, A., Bergman, P., Hjalmarson, A., Friberg, P., Irvine, W. M., Millar, T. J., Ohishi, M., & Saito, S. 1998, *ApJS*, 117, 427
- Nummelin, A., Bergman, P., Hjalmarson, A., Friberg, P., Irvine, W. M., Millar, T. J., Ohishi, M., & Saito, S. 2000, *ApJS*, 128, 213
- Remijan, A., Snyder, L. E., Friedel, D. N., Liu, S.-Y., & Shah, R. Y. 2003, *ApJ*, 590, 314
- Remijan, A., Sutton, E. C., Snyder, L. E., Friedel, D. N., Liu, S.-Y., & Pei, C. C. 2004a, *ApJ*, 606, 917
- Remijan, A., Shiao, Y.-S., Friedel, D. N., Meier, D. S., & Snyder, L. E. 2004b, *ApJ*, 617, 324
- Sault, R. J., Teuben, P. J., & Wright, M. C. H. 1995, in *ASP Conf. Ser. 77, Astronomical Data Analysis Software and Systems IV*, ed. R. A. Shaw, H. E. Payne, & J. J. E. Hayes (San Francisco: ASP), 433
- Stolze, M. & Sutter, D. H. 1985, *Z. Naturforsch.*, 40a, 998
- Tielens, A. G. G. M., & Hagen, W. 1982, *A&A*, 114, 245
- Ulich, B.L., & Haas, R.W. 1976, *ApJS*, 30, 247
- Winnewisser, G., Winnewisser, M., & Christiansen, J. J. 1982, *A&A*, 109, 141
- Woon, D. E., & Dunning, T. H. Jr. 1993, *J. Chem. Physics*, 98, 1358
- Yamada, K. & Winnewisser, M. 1975, *Z. Naturforsch.*, 30a, 672

Table 1. GBT Observations - Cyanide and Isocyanide Molecular Line Parameters and Column Densities

Species	Frequency	Transition	S	E _u	T _c	(+64 km s ⁻¹)		(+73 km s ⁻¹)		(+82 km s ⁻¹)		N _T × 10 ⁻¹³ (cm ⁻²)	N _T (XNC) N _T (XCN)
						(ΔT _A [*]) (mK)	(ΔV) (km/s)	(ΔT _A [*]) (mK)	(ΔV) (km/s)	(ΔT _A [*]) (mK)	(ΔV) (km/s)		
(1)	(2)	(3)	(4)	(5)	(6)	(7)	(8)	(9)	(10)	(11)	(12)	(13)	(14)
CH ₃ CN ^a	18396.7252(7)	1 ₀ -0 ₀	1.332	0.88	10.6	-275(25)	5.8(7)	160(20)	7.9(9)	<7	...		
	18397.9965(6)	1 ₀ -0 ₀	2.220	0.88	10.6	-400(15)	7.0(3)	310(19)	5.9(4)	<7	...	10.8(20)	
	18399.8924(3)	1 ₀ -0 ₀	0.444	0.88	10.6	-180(25)	8.3(9)	<7	...	<7	...		0.02(2)
CH ₃ NC ^b	20105.754(1)	1 ₀ -0 ₀	4.000	0.88	10.2	-48(2)	8.4(4)	11(3)	6.4(9)	<7	...	0.2(1)	
CH ₂ CHCN ^c	18512.158(13)	2 ₁₂ -1 ₁₁	0.375	3.51	11.1	-62(2)	4.9(1)	<7	...	<7	...		
	18513.311(7)	2 ₁₂ -1 ₁₁	0.701	3.51	11.1	-82(2)	4.9(1)	<7	...	<7	...	37.2(30)	
	18514.400(27)	2 ₁₂ -1 ₁₁	0.167	3.51	11.1	-19(3)	4.1(5)	<7	...	<7	...		0.005(2)
CH ₂ CHNC ^d	19993.916(1)	2 ₁₂ -1 ₁₁	1.500	3.67	10.5	8(2)	1.5(4)	<7	...	<7	...	0.2(5)	
CH ₃ CH ₂ CN ^e	18377.721(3)	2 ₁₁ -1 ₁₀	1.500	1.56	10.0	-24(2)	2.8(2)	20(2)	2.8(2)	-20(2)	2.8(2)	3.5(4)	
CH ₃ CH ₂ NC ^f	18803.209(10)	2 ₁₂ -1 ₁₁	1.500	1.56	9.8	<7	...	<7	...	<7	...	<1.1	<0.3
HC ₄ CN ^g	18638.617(2)	7-6	7.000	2.70	10.9	-63(2)	5.8(2)	97(1)	16.0(5)	-59(2)	8.0(3)	6.1(2)	<0.03
HC ₄ NC ^h	19616.504(2)	7-6	7.000	2.84	9.7	<5	...	<5	...	<5	...	<0.2	

Note. — Uncertainties in the frequencies refer to the least significant digit (Taylor & Kuyatt 1994) and are 2 σ values (coverage factor 2). Upper limits of the line intensities are 3 σ values. All other listed uncertainties are 1 σ .

^aRest Frequencies from Boucher et al. 1980; $\mu_a=3.922(1)$ from Gadhi et al. 1984

^bRest Frequencies from Kukolich 1972; $\mu_a=3.830(60)$ from Ghosh et al. 1953

^cRest Frequencies from Gerry et al. 1979; $\mu_a=3.815(12)$, $\mu_b=0.894(68)$ from Stolze, M. & Sutter D. H. 1985

^dRest Frequencies from Yamada & Winnewisser 1975; $\mu_a=3.470(30)$, $\mu_b=0.790(100)$ from Bolton, Owen, & Sheridan 1970

^eRest Frequencies, $\mu_a=3.850(10)$ and $\mu_b=1.230(60)$ from Lovas 1982

^fRest Frequencies from Fliege & Driezler 1985; $\mu_a=3.790(20)$ and $\mu_b=1.310(40)$ from Anderson & Gwinn 1976

^gRest Frequencies from Winnewisser et al. 1982; $\mu_a=4.330(30)$ from Alexander et al. 1976

^hRest Frequencies from Botschwina et al. 1998; $\mu_a=3.590$ calculated in this work

Table 2. BIMA Array Observations - Molecular Line Parameters and Column Densities

Species	Frequency	Transition	$S\mu^2$	E_u	(+64 km s ⁻¹)		(+73 km s ⁻¹)		(+82 km s ⁻¹)		N_T
					(ΔI)	(ΔV)	(ΔI)	(ΔV)	(ΔI)	(ΔV)	
(1)	(MHz)	(3)	(Debye ²)	(K)	(J/bm)	(km/s)	(J/bm)	(km/s)	(J/bm)	(km/s)	(cm ⁻²)
	(2)		(4)	(5)	(6)	(7)	(8)	(9)	(10)	(11)	(12)
H ₂ CCCC ^a	80383.96(2)	9 ₀₉ -8 ₀₈	153.8	19.3	<0.3	...	<0.3	...	<0.3	...	<6.0×10 ¹⁴
HCOOCH ₃ ^b	80395.135(126)	9 ₂₈ -9 ₀₉ E	0.7	28.8	<0.3	...	<0.3	...	<0.3	...	<4.7×10 ¹⁷
CH ₃ CH ₂ CN	80404.898(12)	9 ₂₈ -8 ₂₇	126.1	23.8	4.6(1)	16.0(8)	1.7(3)	5.1(6)	0.6(2)	13.6(4.0)	3.1×10 ¹⁶
CH ₃ NC	80405.504(120)	4 ₃ -3 ₃	29.6	73.0	<0.3	...	<0.3	...	<0.3	...	
CH ₃ NC	80414.660(120)	4 ₂ -3 ₂	50.7	37.4	<0.3	...	<0.3	...	<0.3	...	
CH ₃ NC	80420.062(120)	4 ₁ -3 ₁	63.3	16.0	<0.3	...	<0.3	...	<0.3	...	
CH ₃ NC ^c	80421.910(120)	4 ₀ -3 ₀	67.6	8.9	<0.3	...	<0.3	...	<0.3	...	<4.0×10 ¹³

^aRest Frequency and Line Strength ($S\mu^2$) from Killian et al. 1990

^bRest Frequency and Line Strength ($S\mu^2$) from Bauder 1979

^c N_T calculated using the strongest expected component.

Table 3. Chemical Bonding Energy

Species	ZPCBE ^a	Relative ZPCBE
(1)	(cm ⁻¹)	(cm ⁻¹)
	(2)	(3)
CH ₃ CN	-29,070,027	0
CH ₃ NC	-29,060,541	9,486
CH ₂ CHCN	-37,408,030	0
CH ₂ CHNC	-37,399,372	8,658
CH ₃ CH ₂ CN	-37,672,368	0
CH ₃ CH ₂ NC	-37,663,671	8,697
HC ₄ CN	-53,818,766	0
HC ₄ NC	-53,807,547	11,219

Note. — The Chemical Bonding Energies were Obtained at the MP2/aug-cc-pVTZ Level of Theory (Frisch et al. 2004; Dunning 1989; Kendall, Dunning & Harrison 1992; Woon & Dunning, 1993)

^aZero-Point Corrected Bonding Energy

Fig. 1.— GBT cyanide and isocyanide spectra toward SgrB2(N) at 24.4 kHz channel spacing. Transition quantum numbers are shown in each panel. Each spectrum was processed with a median filter to remove instrumental slopes in the bandpass. The abscissa is the radial velocity with respect to the LSR calculated for the rest frequency of the transition shown (see Table 1) at an assumed source velocity of $+64 \text{ km s}^{-1}$. Dashed lines show LSR velocities at $+64$, $+73$ and $+82 \text{ km s}^{-1}$. In the case of CH_3CN and CH_2CHCN the HF structure is also seen and labeled for an LSR velocity of $+64 \text{ km s}^{-1}$.

Fig. 2.— BIMA array spectral passband toward the LMH hot core of Sgr B2(N) containing the $J_K = 4_K - 3_K$ ($K = 0 - 3$) transitions of CH_3NC . In this case, the rest frequency corresponds to the $\text{CH}_3\text{CH}_2\text{CN}$ transition at 80.4049 GHz for a LSR velocity of $+64 \text{ km s}^{-1}$. However, there are also emission components at $+73$ and $+82 \text{ km s}^{-1}$. Finally, the locations of the transitions of CH_3NC , HCOOCH_3 and H_2CCCC (Table 2) are also labeled assuming an LSR velocity of $+64 \text{ km s}^{-1}$.

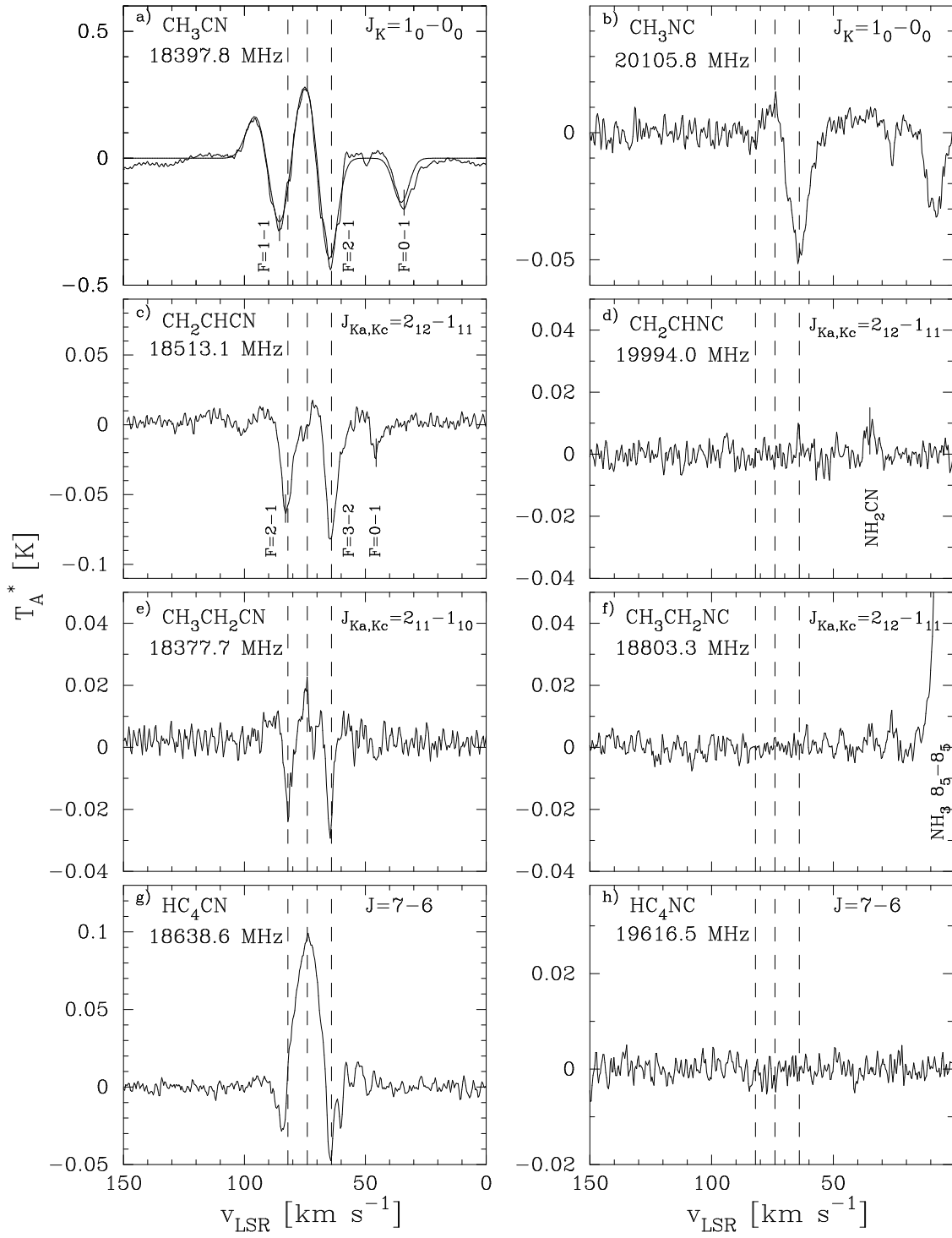


Figure 1.

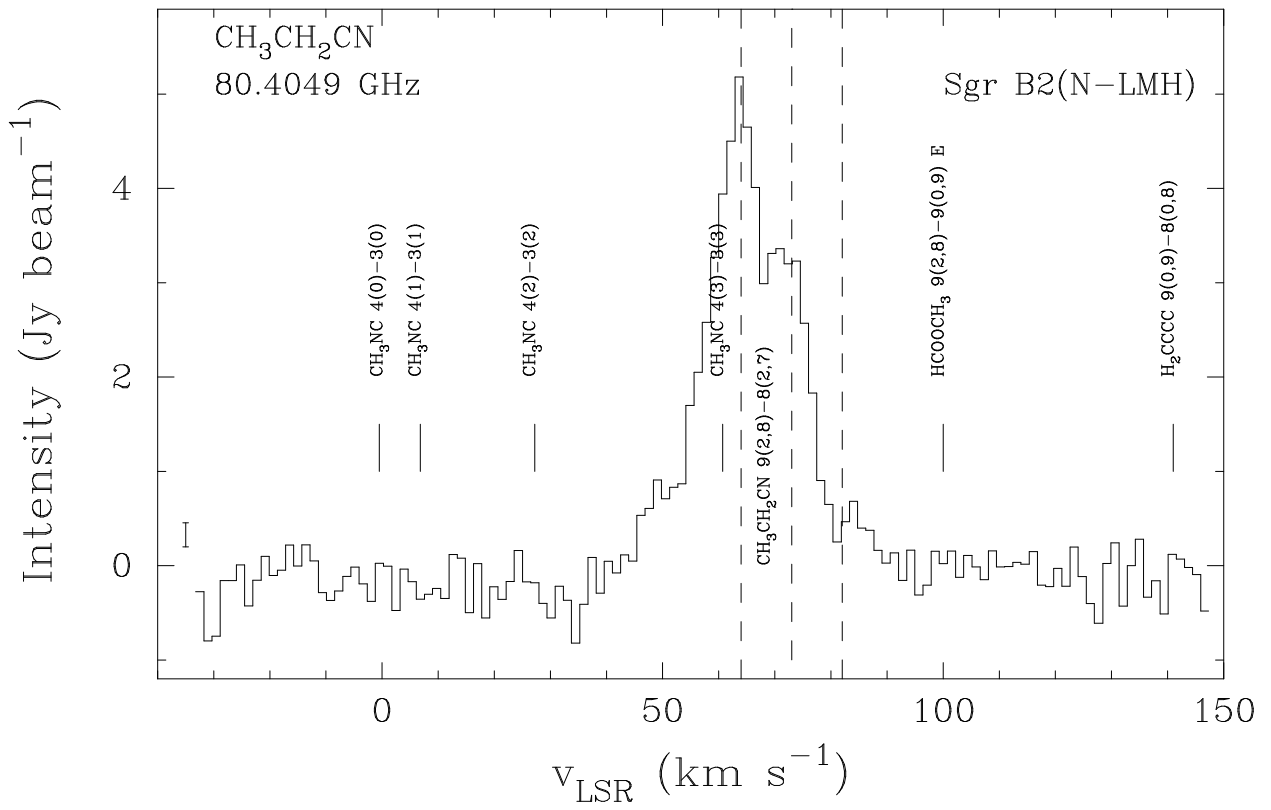


Figure 2.